5-2023

On the Feasibility of Embedding Fe-SMA Short-Fibers in Ultra-High-Performance Concrete for Self Prestressing

Gavin Briggs
University of Arkansas, Fayetteville

On the Feasibility of Embedding Fe-SMA Short-Fibers in Ultra-High-Performance Concrete for Self Prestressing

A thesis submitted in partial fulfillment
of the requirements for the degree of
Master of Science in Civil Engineering

by

Gavin Briggs
University of Arkansas
Bachelor of Science in Civil Engineering, 2021

May 2023
University of Arkansas

This thesis is approved for recommendation to the Graduate Council.

_____
Gary S. Prinz, Ph.D.
Thesis Director

_____
W. Micah Hale, Ph.D.
Committee Member

_____
Cameron Murray, Ph.D.
Committee Member

Abstract

Prestressing concrete is common practice in the construction industry. Current prestressing methods are often used for large, straight members and come with geometric limitations for curved or thin-walled members. Shape memory alloy short fibers embedded within concrete mixes may allow for the prestressing of geometries not possible with traditional methods. This study reviews past research on prestressing concrete with shape memory alloys, evaluates the achievable recovery stress within an Fe-SMA (when deformed at room temperature), and examines the mechanical behavior of Ductal dark grey UHPC when heated to 250 °C. The flexural behavior, compressive strength, and fiber-to-concrete bond strength of heated and non-heated UHPC specimens are investigated to better understand the effect high temperatures on concrete properties. Results from flexure tests indicate heating specimens increases stiffness and modulus of rupture by 6.8% and 28.1 %, respectively. The compressive strength of heated specimens was on average 53.5% higher than non-heated specimens. Steel fiber pullout tests show that fiber-to-concrete bond strength typically increases when specimens are heated to 250 °C. The tests on heated UHPC specimens show that the Ductal mix used behaves favorably upon heating and would likely work well for Fe-SMA prestressing applications. Fe-SMA recovery stress was found to reach approximately 50 ksi. This indicates that Fe-SMA fibers may be able induce about 354 psi of prestress for every 1% (per volume) of Fe-SMA fibers added to a UHPC mix.

Acknowledgments

This study was sponsored by the US Army Corps of Engineers. We acknowledge and are grateful for the funding and assistance provided by the Corps. Tests in this study were conducted in the Grady E. Harvell Civil Engineering Research and Education Center (HCEC) at the University of Arkansas. I would like to thank many people for their advice and assistance with testing, including: Mark Kuss, Daniel Davidson, Charissa Puttbach, Bezhad Farivar, Lane Edwards, Andres Calzacorta, Paul Chabaud and Rilye Dillard. I would also like to thank Dr. Cameron Murray and Dr. Micah Hale for their guidance and service on my committee.

Table of Contents

List of Tables

List of Figures

1. Introduction

Concrete typically has greater strength in compression than in tension. For this reason, steel is often used as tensile reinforcement within concrete structures. Member strains great enough to develop considerable tension in the reinforcing steel may also initiate cracking of the concrete. Cracking may allow for the infiltration of water and other corrosive solutions which could reduce the service life of a member. To delay crack formation, reinforcing steel can be prestressed to mobilize the tensile strength of the steel before crack initiation.

Compressive pre-stressing of concrete materials can increase relative tensile capacity (through a shift in stress-state) [resulting in improved performance under flexural and tensile loading] without a negative effect on overall material behavior, because concrete materials typically have higher strength in compression than tension. Material prestress is commonly induced through mechanical processes (the embedment of pre-stressed strands or installation of post-tensioned elements following concrete curing). Mechanical prestressing is labor-intensive and often requires specialized equipment. Mechanical prestressing is typically used for large, straight concrete members [2] and is not suitable for curved or thin-walled members [3]. Methods that induce concrete prestress while overcoming the fabrication and geometry limitations mentioned are desirable.

Shape memory alloys (SMAs) have the potential to induce prestress using their shape memory effect (SME) (Figure 1). Once axially strained/stretched, SMAs can be heated, causing the material to recover its original shape via the SME. If this shape recovery is prevented by some form of restraint, a recovery stress develops within the material as it tries to contract. If axially strained fibers are embedded in cured concrete, then upon heating, the fibers will develop recovery stress which may be transferred to the surrounding concrete as a compressive force.

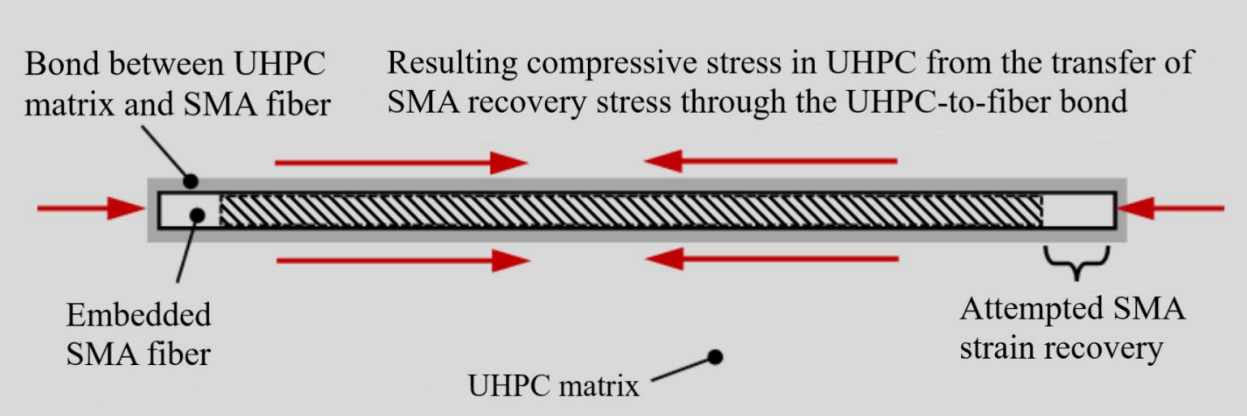

Figure 1. Prestressing effect of SMA fibers

1.1 Background of Related Research

In 2005, Moser, Bergamini, Christen, and Czaderski investigated nickel and titanium-based shape memory alloy (NiTi alloy) short fibers as a method of prestressing concrete and found that shape memory alloys (SMA's) can induce prestress. After being strained, these NiTi alloy fibers can be heated to induce a shape memory effect (SME) resulting in the fibers contracting to their original length. When this contraction is not allowed due to some form of constraint, internal tensile stress develops within the fiber. If the fibers are constrained by a mortar matrix, this internal tensile stress within the fiber will be transferred to the surrounding matrix as an internal compressive stress.

Moser et al. (2005) produced mortar prisms containing pre-strained loop and star NiTi alloy fibers (Figure 2) along with control specimens without fibers.

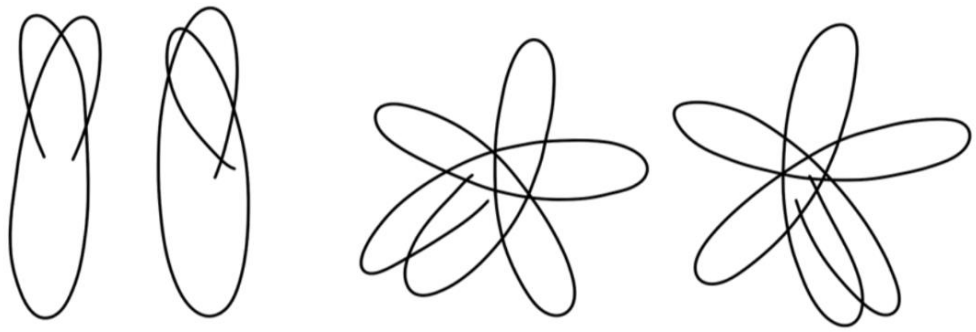

Loop-fibers Star-Fibers

Figure 2. Fiber shapes [7] (shapes have been redrawn for clarity)

These specimens were heated to various temperatures while monitoring strain. When heated, all specimens experienced strain due to expansion. Fiber-reinforced specimens had less strain because while the mortar expanded it was partially restricted by the contraction of the NiTi alloy fibers (Figure 3).

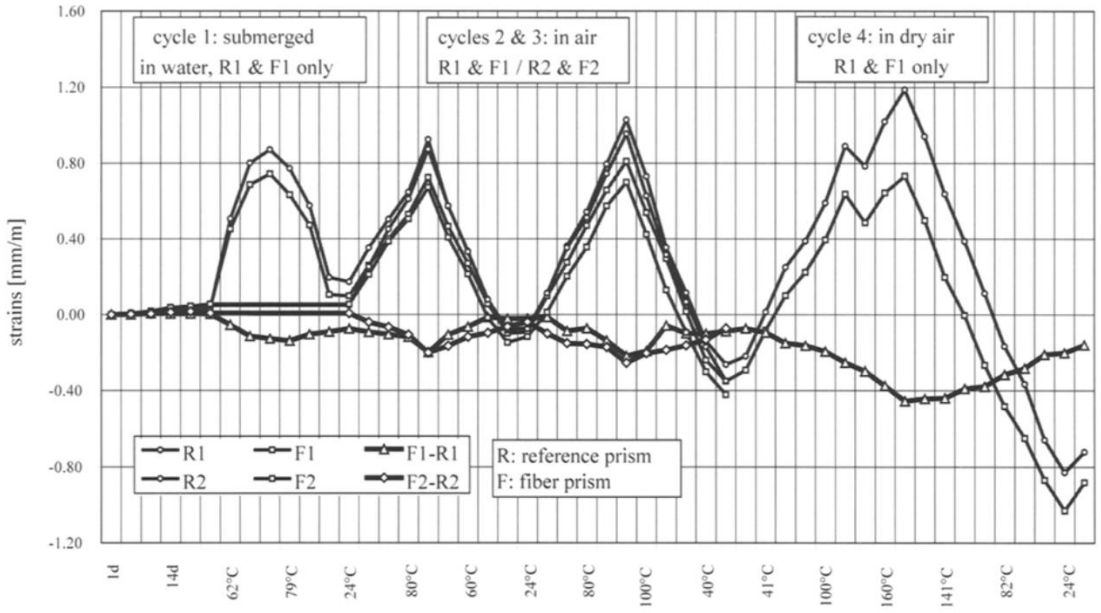

Figure 3. Strains of mortar prisms during temperature cycles by Moser et al. 2005

The difference in strain between control and reinforced prisms was considered to be due to prestress. Based on this difference, prestress induced by NiTi alloy fibers was estimated at about 7 MPa or 1015 psi. Specimens in this experiment were heated to a maximum temperature of 180 °C. This temperature was found to cause little microcracking in the mortar as the elastic modulus was reduced by only about 10%. Additionally, the difference in the coefficient of thermal expansion between the mortar and NiTi alloy was determined to be negligible.

While this study found that NiTi alloy fibers can induce substantial prestress, the cost was said to be too high for practical application. Additionally, the looped shape of the fibers may cause issues with workability therefore alternative fiber geometries should be explored.

In 2009, Orvis researched the feasibility of prestressing concrete using NiTi alloy fibers with a geometry like traditional steel fibers. Short fibers may be able to prestress curved or thin-walled members in which long wires would not be practical [8]. This study found that these SMA fibers can induce a prestressing force, but this force varied greatly, and further research would be needed to find an effective way to prestress with NiTi alloys.

The SMA fibers had diameters of 0.04” and 0.075”, were randomly distributed in the mortar samples, and had hooked ends to provide anchorage (Figure 4). This hooked anchorage was found to be flawed because when they were heated, the hooks tried to straighten which increased stress within the concrete sample [8].

Figure 4. Hooked NiTi alloy fibers by Orvis 2009

Orvis also considered prestressing losses. Once a member is prestressed, losses begin to occur. These losses can be attributed to the shortening of the concrete member in the direction of prestressing tendons which allows for additional relaxation of the SMA fibers. Shortening of the concrete can be caused by creep, shrinkage, or elastic shortening. Additionally, prestress can be lost due to insufficient bondage between NiTi alloy fibers and the surrounding matrix which would result in less force transfer from the fiber to the concrete. In this study, only two of the six specimens with discrete, randomly distributed SMA fibers resulted in any prestressing force. This was believed to be caused by the concrete being weakened from exposure to high temperatures, cracking within the interfacial transition zone around the fibers, the added stress due to the hooked ends straightening, or a combination of these issues. NiTi alloy can prestress concrete but due to high cost and variability within samples, it does not seem like a realistic method of prestressing [8].

In 2013, Lee, Weber, Feltrin, Czaderski, Motavalli, and Leinenbach investigated the phase transformation behavior of an iron-based shape memory alloy (Fe-SMA). This material is cheaper than NiTi-based SMA's and may have practical applications for prestressing concrete.

The shape-memory-effect (SME) of Fe-SMA's is caused by stress and heat-induced phase changes [5]. Fe-SMA's begin mostly in the austenite phase and when deformed some of these austenite grains change to martensite. Upon heating, a reverse transformation occurs, and the newly formed martensite grains revert to the austenite phase. The shift from martensite back to austenite causes the Fe-SMA to recover its original shape (referred to as recovery strain).

Lee et al. confirmed that Fe-SMA's consist mostly of austenite grains before deformation. Once samples were strained to 4%, the concentration of martensite grains increased. Samples in this study were deformed at -45 °C and 100 °C to examine the effect of deformation temperature on stress-induced martensitic phase transformation. It was determined that the martensite phase is formed more easily at low temperatures. These results are shown in Figure 5. The austenite phase appears brown, and the martensite is shown in white.

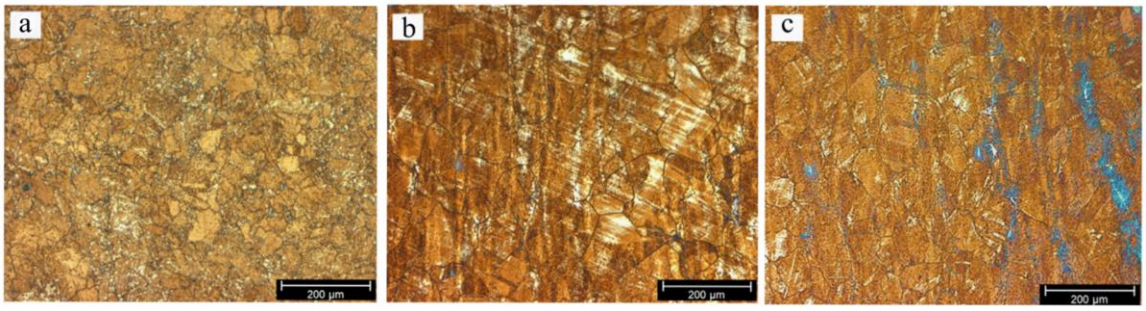

Figure 5. Fe-SMA samples before and after deformations (a) undeformed sample (b) sample deformed at -45 °C (c) sample deformed at 100 °C by Lee et al. 2013

Fig. 4a shows an undeformed sample consisting mostly of austenite grains with some martensite grains present. Martensite was believed to be formed by internal stress from differential thermal expansion during manufacturing. Fig. 4b shows a sample after being deformed at -45 °C. In this image, the concentration of martensite has increased in comparison to Fig. 4a. Fig. 4c shows a sample after being deformed at 100 °C. Although the concentration of martensite in this sample has increased in comparison to the undeformed sample, more is present in the sample deformed at -45 °C indicating that lower deformation temperatures facilitate martensite formation.

Samples were strained at various temperatures and then heated to 200 °C. It was found that recovery strain decreased with an increase in deformation temperature. This is due to the decrease in martensite formation with an increase in deformation temperature. The recovery strain caused by heating was also examined (Figure 6). Specimens were strained to 4% at -45 °C, held at various stresses, and then heated to 200 °C to induce the SME.

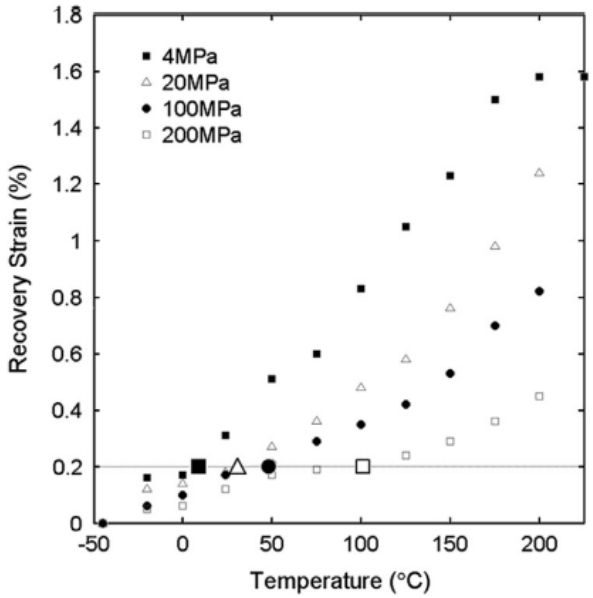

Figure 6. Change in recovery strain upon heating by Lee et al. 2013

These results show that recovery strain increases with an increase in activation temperature. It was found that, when deformed at -45 °C, there is little increase in recovery strain when heated beyond 200 °C.

Although these results are useful in understanding the behavior of this Fe-SMA, a deformation temperature of -45 °C would be difficult to implement in practice without some premature recovery strain due to exposure to ambient temperatures and concrete heat of hydration. Therefore, material behavior after being deformed at room temperature should be explored. Additionally, an analysis of material behavior upon cooling would be useful in design.

In 2020, Choi, Ostadrahimi, Kim, and Seo investigated the prestressing effect of iron-based shape memory alloy (Fe-SMA) wires on the flexural behavior of mortar beams. They found that Fe-SMA prestressing wires delayed cracking force, increased ductility, and increased stiffness when compared to a non-heated reinforced beam. Like NiTi-SMA's, Fe-SMA's can be strained and then heated to recover their original shape, and if restrained when heated (Figure 7), internal tensile stresses (recovery stresses) will develop within the SMA.

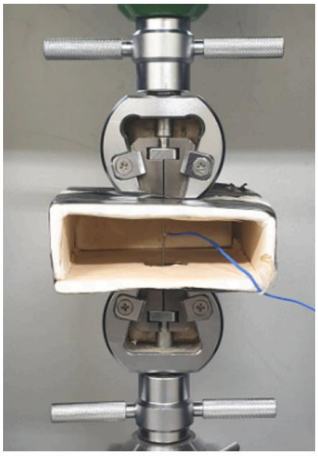

Figure 7. Experimental setup to measure recovery stress within the Fe-SMA by Choi et al. 2020

This study explored the variance of recovery stress with temperature and prestrain. Choi et al. determined that final recovery stress increases with an increase in activation temperature (Figure 8). When wires with prestrains of 4%, 5%, and 6% were tested, it was found that final recovery stress decreases with increasing prestrain (Figure 9). To study the prestressing effects of the Fe-SMA in mortar beams, 18 Fe-SMA wires with diameters of 0.7 mm prestrained 5% were placed longitudinally in the bottom of a 30 mm wide by 20 mm deep mortar beam for a Fe-SMA content of 1.15% by volume. Once the mortar cured, the specimen was heated to a temperature of 300 °C. Specimens were then loaded in three-point bending tests (Figure 10).

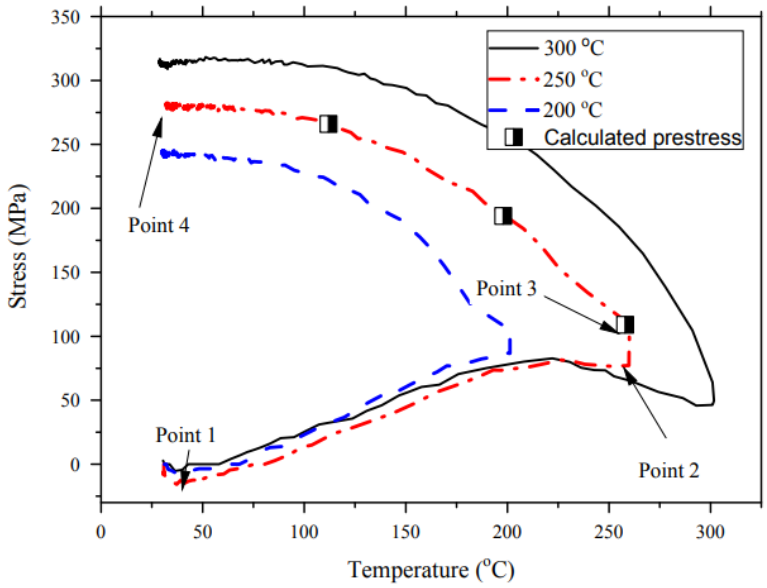

Figure 8. Recovery stress at various temperatures using 5% prestrained Fe-SMA wire by Choi et al. 2020

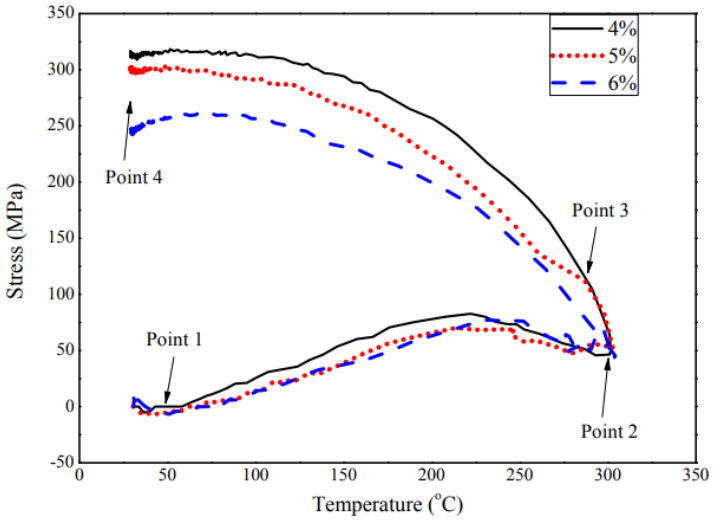

Figure 9. Recovery stress for differently prestrained Fe-SMA wire at 250°C by Choi et al. 2020

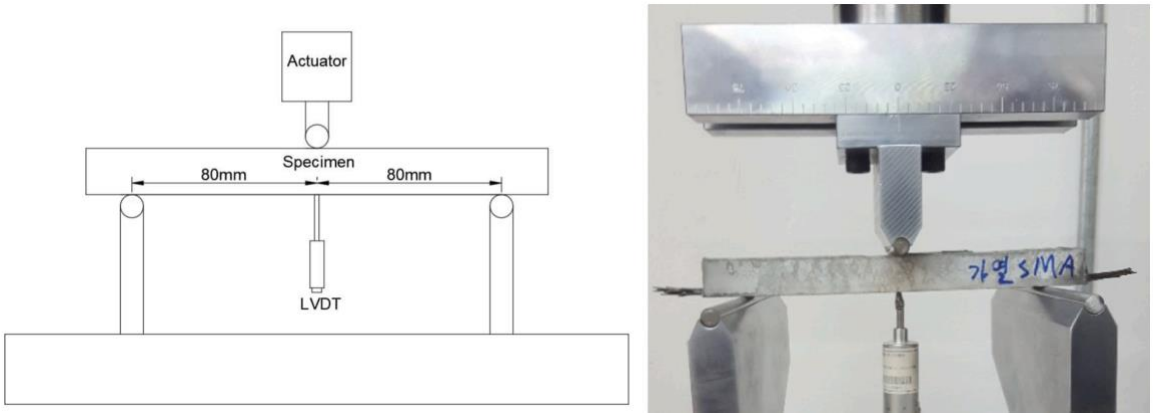

Figure 10. Experimental setup for three-point bending test by Choi et al. 2020

Three Fe-SMA reinforced specimens (R1, R2, and R3) were tested. R1 and R2 were heated and R3 was not. Bending tests showed that heated specimens were stiffer and could withstand more load before cracking than non-heated specimens. At failure, the heated specimens deflected about twice as much as the non-heated specimen (Figure 11).

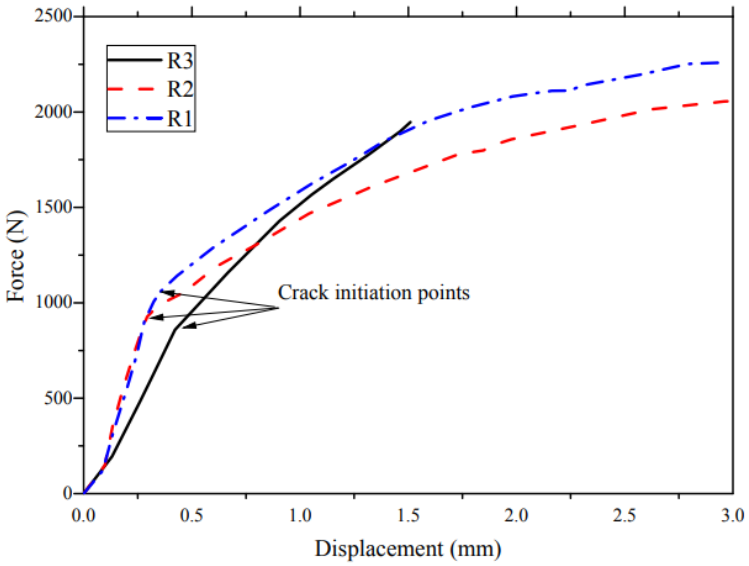

Figure 11. Force-displacement diagram for heated (R1 and R2) and non-heated reinforced beam (R3) by Choi et al. 2020

The results of this study indicate that Fe-SMA wires were able to induce significant prestressing forces on mortar specimens, but the prestressing effect of short Fe-SMA fibers was not considered.

Because activation of the shape memory effect of Fe-SMA's requires the material to be heated to temperatures up to 300 °C [2], the effect of these high temperatures on the concrete must also be considered. In 2014, Ma, Guo, Zhao, Lin, and He conducted a review of the mechanical properties of concrete at high temperatures. The results of this review indicate that when exposed to high temperatures, most concrete mechanical properties deteriorate. Unlike most other properties, concrete compressive strength remains unchanged or even increases when exposed to temperatures up to 300 °C (Figure 12). Flexural strength, tensile strength, and modulus of elasticity of concrete decrease with an increase in temperature at an almost linear rate (Figures 13-15).

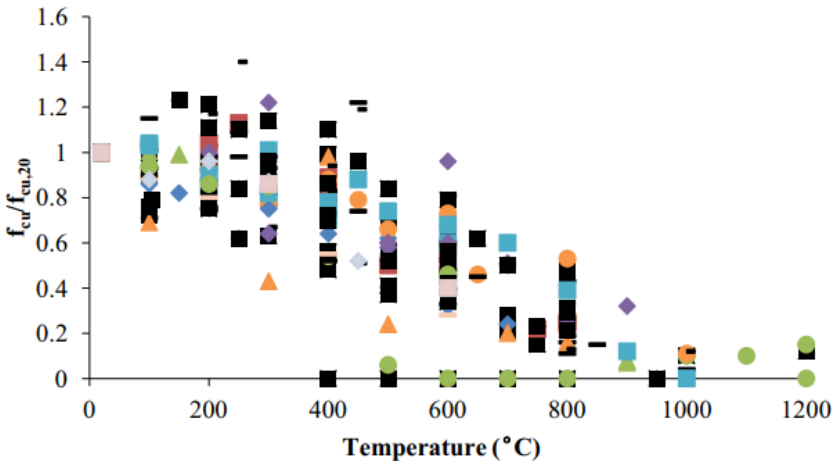

Figure 12. Residual compressive strength of concrete at elevated temperatures by Ma et al. 2014 [for legend see Mechanical Properties of Concrete at High Temperature—A review By Ma, Guo, Zhao, Lin, and He (2014)]

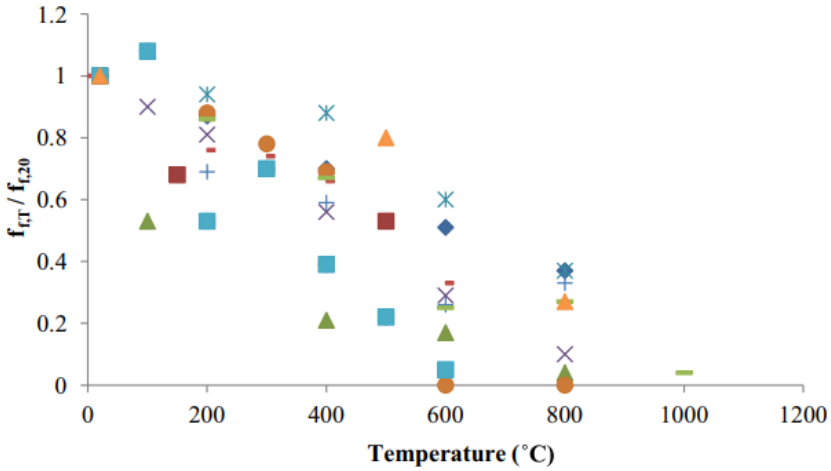

Figure 13. Residual flexural strength of concrete at elevated temperatures by Ma et al. 2014 [for legend see Mechanical Properties of Concrete at High Temperature—A review By Ma, Guo, Zhao, Lin, and He (2014)]

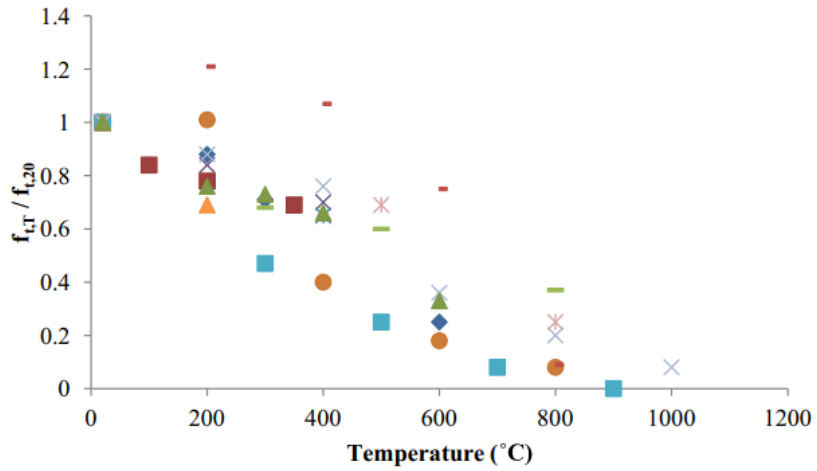

Figure 14. Residual splitting tensile strength of concrete at elevated temperatures by Ma et al. 2014 [for legend see Mechanical Properties of Concrete at High Temperature—A review By Ma, Guo, Zhao, Lin, and He (2014)]

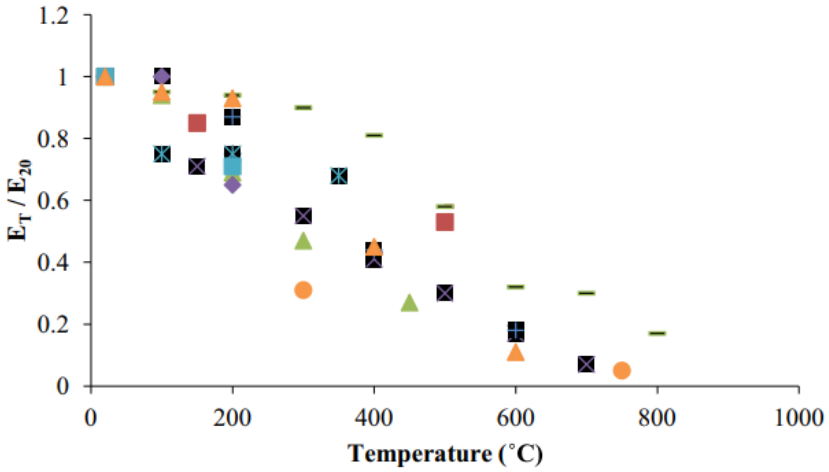

Figure 15. Residual modulus of elasticity of concrete at elevated temperatures by Ma et al. 2014 [for legend see Mechanical Properties of Concrete at High Temperature—A review By Ma, Guo, Zhao, Lin, and He (2014)]

Results of this review indicate that the mechanical properties of concrete typically diminish with elevated temperature but, the extent of deterioration varies widely with different

concrete mixes. To understand the mechanical behavior of a specific mix after being exposed to high temperatures it should be tested directly.

1.2 Summary of Related Research

In 2005, Moser, Bergamini, Christen, and Czaderski investigated nickel and titanium-based shape memory alloy (NiTi alloy) short fibers as a method of prestressing concrete. Although this study proved that the shape memory effect is capable of prestressing concrete, the fibers manufactured by Moser et al. had a geometry that may cause issues in practical applications. In 2009, Orvis researched the feasibility of prestressing concrete using NiTi alloy fibers with geometries like traditional steel fibers and found (with variability) that these fibers could induce prestress. Both studies concluded that although nickel and titanium-based shape memory alloys can induce prestress, their application is impractical due to high cost.

In 2013, Lee, Weber, Feltrin, Czaderski, Motavalli, and Leinenbach investigated the phase transformation behavior of an iron-based shape memory alloy (Fe-SMA). This study provides an in-depth look at the phase behavior of an Fe-SMA and concludes that the alloy's properties may allow for prestressing concrete at a lower cost than NiTi-SMA's. Lee et al. did not report SMA stress upon cooling (after activation) which is crucial for estimating lasting prestressing effects.

In 2020, Choi, Ostadrahimi, Kim, and Seo investigated the prestressing effect of Fe-SMA wires on the flexural behavior of mortar beams. They found that Fe-SMA prestressing wires delayed cracking force, increased ductility, and increased stiffness when compared to a non-heated reinforced beam. This study confirmed that Fe-SMA's can induce prestress at a lower price than NiTi-SMA's, but it did not investigate the prestressing effect of short Fe-SMA fibers.

Activation temperatures up to 300 °C are required for Fe-SMA's and therefore the effect that high temperature exposure may have on concrete must be considered. Ma, Guo, Zhao, Lin, and He conducted a review of the mechanical properties of concrete at high temperatures and found that the flexural capacity of most concrete decreases with an increase in temperature. The rate of deterioration varies with mix designs. Because of this variation, the flexural behavior of the specific concrete mix (after being exposed to Fe-SMA activation temperatures) should be evaluated to best quantify the prestressing effect of an Fe-SMA.

The aim of this study is to assess the feasibility of prestressing UHPC with Fe-SMA short fibers by investigating individual factors. The change in concrete mechanical properties and concrete-to-fiber bond strength after exposure to a potential SME activation temperature (250 °C) is examined. Additionally, the residual recovery stress of an Fe–17Mn–5Si–10Cr–4Ni–1(V,C) (ma.-%) SMA upon cooling is defined (when deformed at room temperature). These investigations help understand the factors that affect prestress and the interaction between components of Fe-SMA prestressed UHPC.

2 Proposed Method for Achieving Internal Prestress

Due to product acquisition issues and local manufacturing limits, this study was done without the desired short Fe-SMA fibers. A method for inducing prestress using Fe-SMA short fibers (Figure 16) has been detailed and will be implemented in future research. Prestress may be achieved by adding prestrained (axially stretched) Fe-SMA short fibers to a UHPC mix. After curing, the mix can be heated to induce the SME of the fibers. As the fibers try to contract, the force they exert will be transferred to the confining concrete (assuming the fiber-to-concrete bond is strong enough), resulting in compressive stress within the matrix. The variation of

recovery stress with temperature and pre-strain is predictable [2, 4] and may allow for tunable levels of prestress based on recovery temperature, pre-strain, and SMA fiber content.

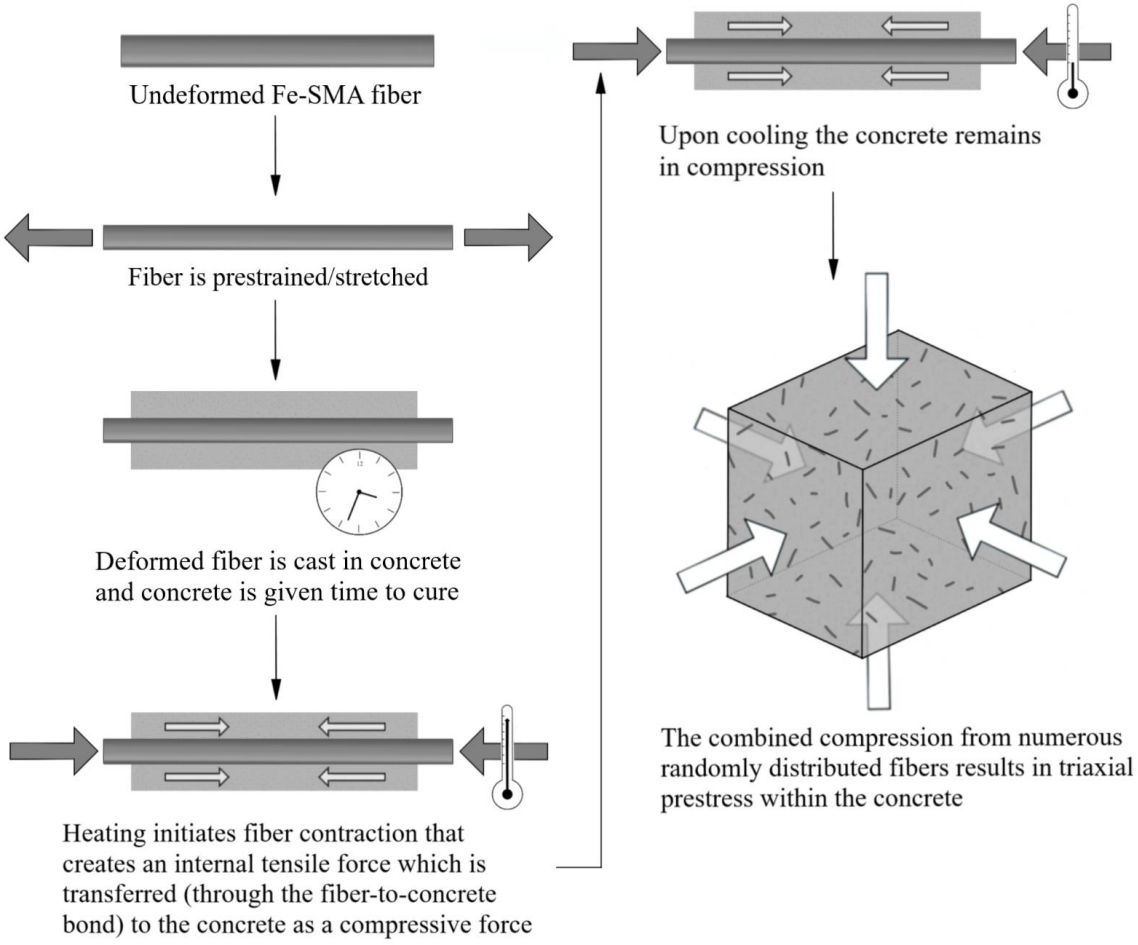

Figure 16. Method for prestressing using Fe-SMA short fibers

Along with this method, the derivation for an equation (like the equation used by [7]) that estimates achievable prestress based on SMA fiber content and recovery stress has been included. The force generated by the SME of an individual fiber (F_f) is the product of the fiber recovery stress (σ_f) and the cross-sectional area of the fiber (A_f), as shown in Equation 1. The total force exerted by the SME of the fibers (ΣF_f) is then the product of the sum of fiber areas (ΣA_f) and the recovery stress, as shown in Equation 2. Assuming a complete force transfer from

the fibers to the concrete, Equation 3 shows that the compressive stress within the concrete (σ_c) is the total force exerted by the SME of the fibers (adjusted by a factor of 0.71 to account for average fiber orientation with respect to a potential crack – see Figure 17) divided by the cross-sectional area of concrete (A_c). By substituting Equation 2 in for ΣF_f in Equation 3, the compressive stress within the concrete can be written as shown in Equation 4. Due to the random distribution and orientation of fibers, the ratio of the sum of fiber areas to the cross-sectional area of concrete ($\frac{\Sigma A_f}{A_c}$) is equal to the percentage of fibers by volume (ρ) (represented by Equation 5). By substituting ρ in for $\frac{\Sigma A_f}{A_c}$ in Equation 4, the compressive stress (prestress) within the concrete based on fiber content and recovery stress can be written as shown in Equation 6.

$$F_f = \sigma_f \cdot A_f \qquad \text{(Eq. 1)}$$

$$\Sigma F_f = \sigma_f \cdot \Sigma A_f \qquad \text{(Eq. 2)}$$

$$\sigma_c = \frac{0.71 \cdot \Sigma F_f}{A_c} \qquad \text{(Eq. 3)}$$

$$\sigma_c = \frac{0.71 \cdot \sigma_f \cdot \Sigma A_f}{A_c} \qquad \text{(Eq. 4)}$$

$$\frac{\Sigma A_f}{A_c} = \rho \qquad \text{(Eq. 5)}$$

$$\sigma_c = 0.71 \cdot \sigma_f \cdot \rho \qquad \text{(Eq. 6)}$$

This estimation essentially distributes the stress within the Fe-SMA fibers over an area of concrete. These calculations assume random fiber distribution and adequate fiber embedment depth/bond to resist fiber-to-concrete interface separation. Creep, shrinkage, and elastic shortening of concrete were ignored in the development of this equation. These factors could

lower the achievable prestress due to a reduction in recovery stress caused by the shortening of Fe-SMA fibers [8]. The effect of these factors can be more easily understood with empirical data and should be explored in future studies to accurately estimate prestress.

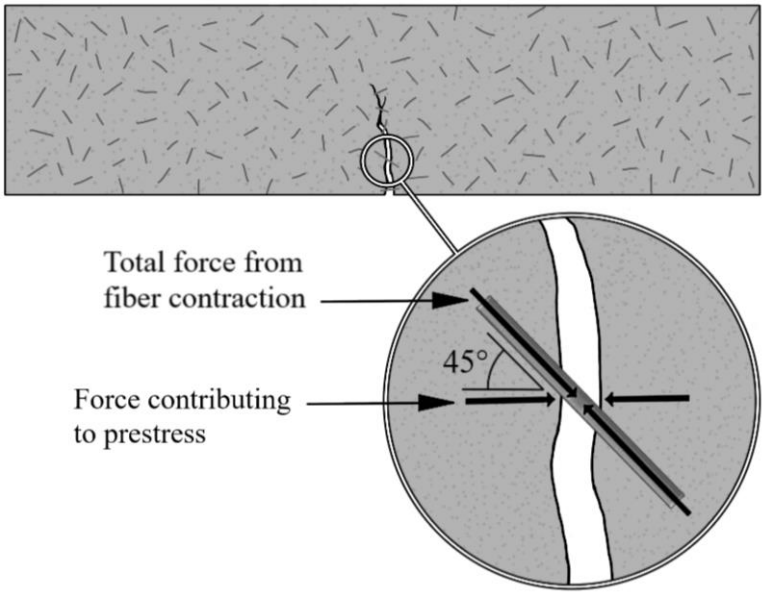

Figure 17. Influence of fiber angle on prestress

3 Experimental Study

To estimate achievable prestress from Fe-SMA fibers more accurately, Fe-SMA behavior and concrete performance after exposure to an activation temperature of 250 °C were investigated. Tests on heated and non-heated UHPC specimens were conducted to understand the effect heating has on a specific UHPC mix design and assess whether the mix could be suitable for Fe-SMA prestressing applications. All specimens used in this study were made using the same mix design and mixing procedure. 25 lbs of Ductal dark gray dry mix was mixed with 800 grams of water and 155 grams of Plastol high-range-water-reducer. No fibers were added. Once hardened, specimens cured at 22 °C in a dry environmental chamber. After 7 days of curing, heated specimens were placed in a room temperature oven and heated to the target temperature

of 250 °C. After 4 hours of heating, the oven was shut off and given time to cool back to room temperature. Dry curing and gradual temperature change reduced the likelihood of explosive spalling [11]. Upon cooling, they were placed back in a dry environmental chamber until they reached the age of 14 days, when they were tested alongside the non-heated specimens.

Initial testing was conducted to determine the time required for a UHPC specimen to reach at least 250 °C. Third-point flexural tests, compressive tests, and steel fiber pullout tests were performed on both heated and non-heated specimens. These tests were conducted to quantify the change (due to heating) in flexural capacity, stiffness, compressive strength, and fiber-to-concrete bond strength. An 18 mm diameter Fe-SMA rod (produced by re-fer AG Company in Switzerland) was tested to validate the recovery stress of the material and facilitate prestress estimation.

3.1 Specimen Heating

For this test, a 4 by 4 by 16 in. UHPC specimen (the largest specimen used in this study) was cast with a thermocouple wire set in the center to measure temperature change over time. After 7 days of curing in a dry environmental chamber at 22 °C, the specimen was placed in a Yamato DVS400 gravity convection oven which then began heating to 250 °C. The specimen reached the target internal temperature in about 3 hours and 40 minutes (Figure 18). For all other tests, oven time was set to 4 hours to ensure specimens were thoroughly heated.

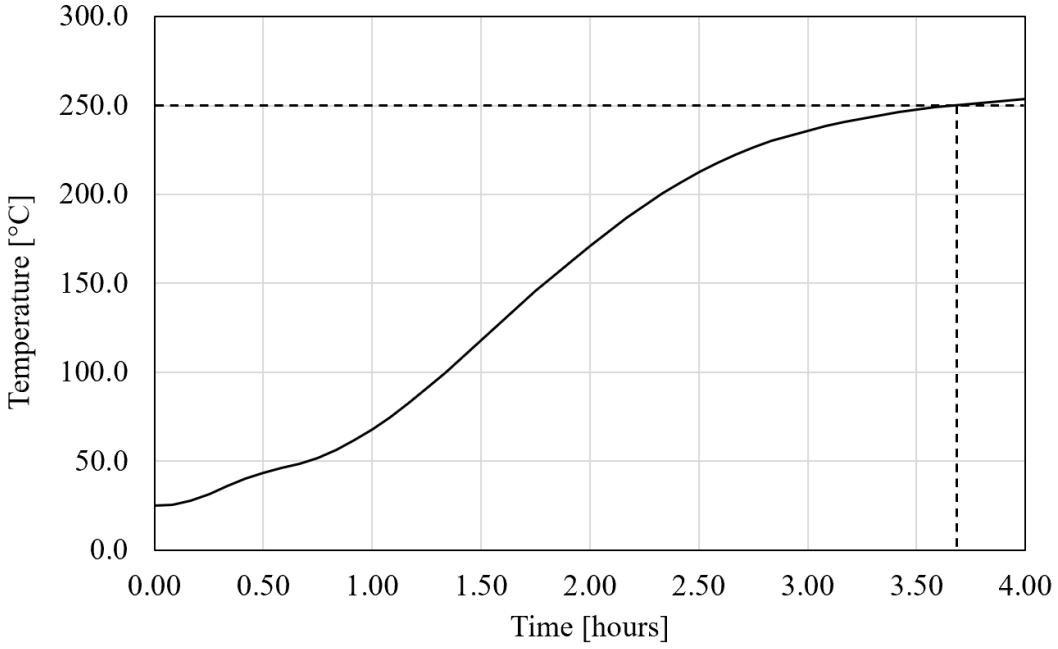

Figure 18. Rate of temperature gain for 4 by 4 by 16 in. UHPC specimen

3.2 Flexure Tests

Third-point flexure tests were conducted on 7 heated and 7 non-heated 4 by 4 by 16 in. specimens. To mitigate the potential influence of varying curing conditions, specimens were made in pairs in which one would be heated, and one would be left unheated. Flexure tests were performed in partial accordance with ASTM C1609 using a Walter + Bai Servohydraulic Biaxial Fatigue Testing Machine at a load rate of 0.002 inches per minute. The specimen span length was 12 inches with equal loads applied at third points (See Figure 19 for test schematic, shear, and moment diagrams). This configuration ensures that rupture will be entirely due to bending stresses if it occurs within the middle third of the specimen. Load (P) and deflection at the third points (Δ) were recorded until rupture. Cross-sectional measurements were taken at the point of fracture to calculate the approximate moment of inertia (I) of individual specimens. The

stiffness (E) and modulus of rupture (σ_t) were then calculated using Equation 7 [1] and Equation 8.

$$E = \frac{160P}{3\Delta I} \qquad \text{(Eq. 7)}$$

$$\sigma_t = \frac{8P}{I} \qquad \text{(Eq. 8)}$$

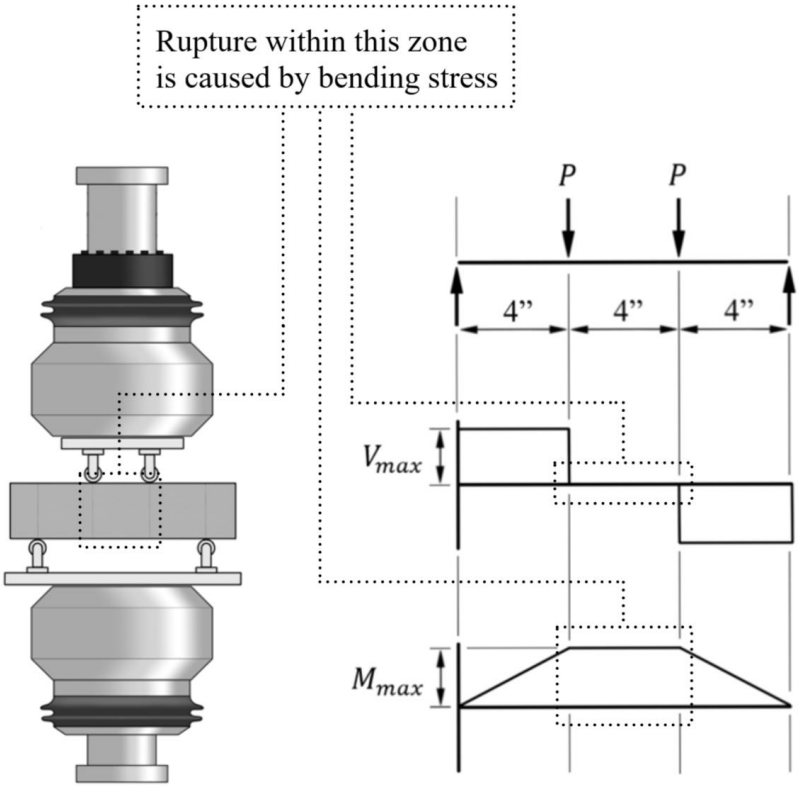

Figure 19. Flexure test schematic and loading diagrams

3.3 Compression Tests

SMA prestressing fibers may increase relative concrete tensile strength, but they can also decrease relative compressive strength (when compared to traditional steel fiber reinforced concrete). Therefore, concrete compressive behavior after heating should be considered. Compression tests were performed on 2 by 2 by 2 in. in a Forney 400 Series Compression

Machine at a ramp rate of 75 psi/sec. These cubes were tested to quantify the difference in strength between heated and non-heated specimens and to compare flexure specimen mixes. When a flexure specimen was made, 3 cubes were cast using the same mix. If the flexure specimen was heated the respective cubes were as well.

3.4 Fiber Pull-Out Tests

Steel fiber pull-out tests were conducted on 2 by 2 by 2 in. specimens to examine the effect heating may have on fiber-to-concrete bond strength. Straight steel fibers with no anchorage were used to ensure pull-out resistance is from bond strength. 36 total specimens were cast with 0.039 in. (1 mm) diameter steel fibers at embedment depths of 0.25, 0.5, and 0.75 in (Figure 20) under two different heating conditions (heated and non-heated). Table 1 provides a summary of pull-out specimens. All fiber pull-out specimens were made from the same batch of concrete to avoid variance in mixing and curing conditions.

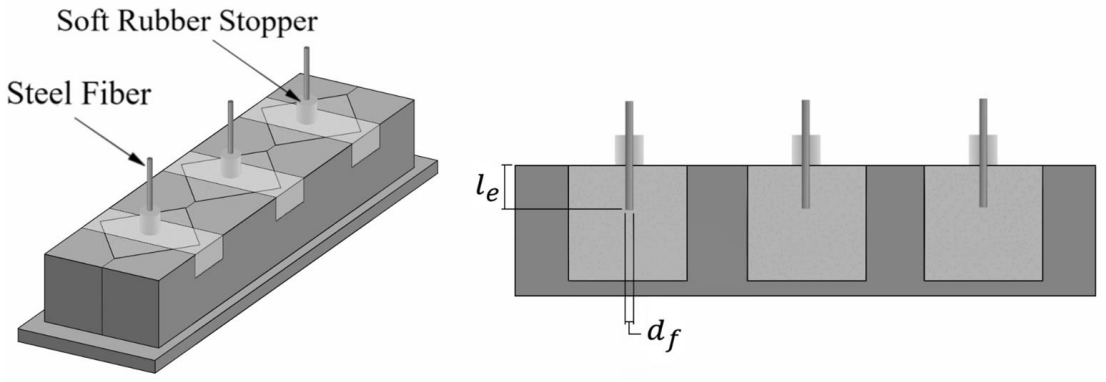

Figure 20. Pull-out specimen fabrication (not to scale)

Table 1. Pull-out Specimen Summary

		Fiber Embedment Depth		
		0.25 in.	0.50 in.	0.75 in.
Number of Specimens	**Heated**	6	6	6
	Non-heated	6	6	6

After 14 days of curing, specimens were restrained in an MTS machine, and fibers were loaded in tension until pull-out occurred (See Figure 21 for test schematic). Maximum pull-out force before slippage was recorded for each test. If the fiber did not rupture before slippage occurred, all pull-out resistance would be due to bond strength [9]. Bond strength (τ_f) was determined by dividing the maximum pull-out force (P_f) by the area (excluding fiber tip area) of fiber in contact with concrete as shown in Equation 9.

$$\tau_f = \frac{P_f}{\pi d_f l_e} \qquad \text{(Eq. 9)}$$

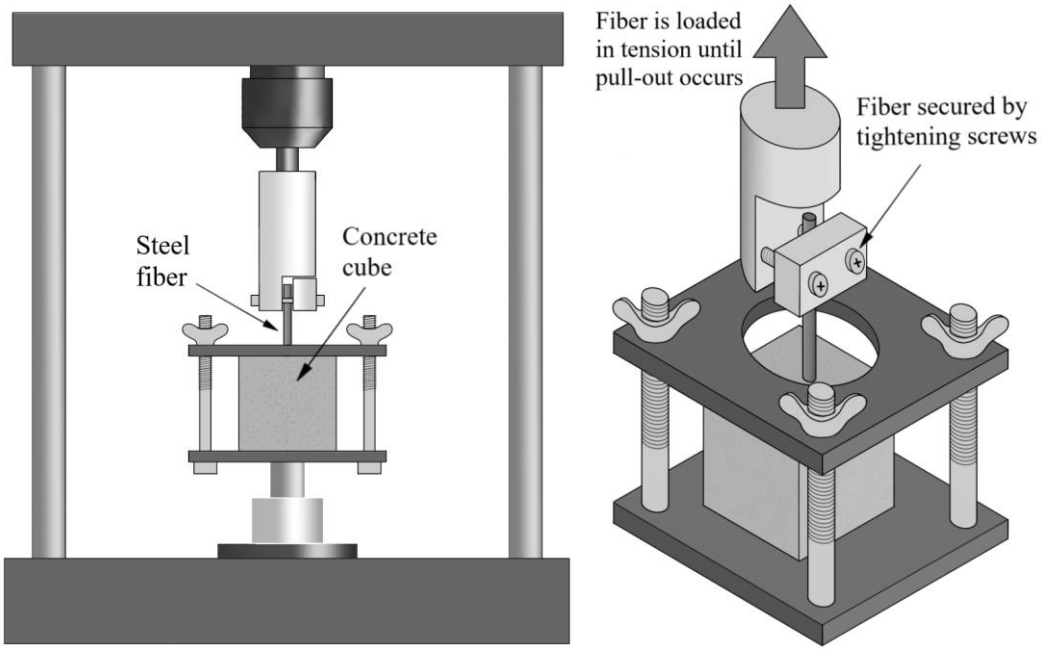

Figure 21. Fiber pull-out test schematic (not to scale)

A theoretical equation for determining the required fiber embedment length (l_e) (Total fiber length in application would need to be twice the required embedment length) to resist recovery stress induced fiber-to-concrete interface separation has also been developed. By setting Equation 1 equal to the pull-out force in a rewritten form of equation 9 and simplifying, Equation 10 is found.

$$P_f = \frac{\tau_f}{\pi d_f l_e} \qquad \text{(Eq. 9 rewritten)}$$

$$l_e = \frac{\sigma_f d_f}{4\tau_f} \qquad \text{(Eq. 10)}$$

3.5 Fe-SMA Material Behavior

To better estimate achievable prestress, the recovery stress of the Fe–17Mn–5Si–10Cr–4Ni–1(V,C) (ma.-%) SMA (produced by re-fer AG Company in Switzerland) was investigated. For this test, an 18 mm. diameter Fe-SMA rod was axially strained 6% (at a rate of 0.1 mm/sec or 0.00394 in/sec) at room temperature in a Walter + Bai Servohydraulic Biaxial Fatigue Testing Machine. After prestraining, the rod was unloaded at the same rate until the internal tension was reduced to approximately 7500 psi (to prevent buckling from thermal expansion [2, 4]). Two Type K thermocouple wires were secured to the rod (using thermal insulating tape) to measure temperature throughout the test. It was then heated to the target temperature of 250 °C using a hand torch. Internal tension within the rod during and after heating/cooling was measured (using the load cell in the fatigue testing machine) to determine recovery stress. A test schematic is shown in Figure 22.

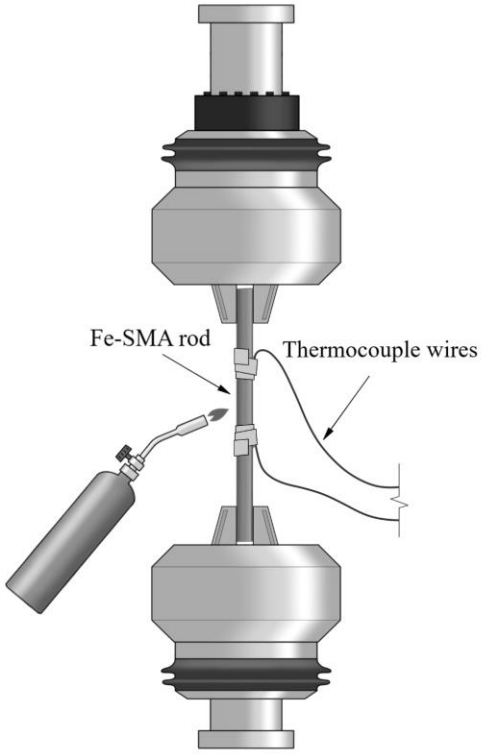

Figure 22. Fe-SMA recovery stress test schematic (not to scale)

4 Experimental Results and Discussion

4.1 General Heated UHPC Behavior

The investigated mechanical properties of this concrete mix were found to improve (on average) when specimens were exposed to the activation temperature of 250 °C (likely due to cement rehydration by free water that is evaporated during heating [10]). A complete set of flexural and compressive test results are displayed in Table 2 (Specimens labeled H have been heated and those labeled NH have not been heated). Change in mechanical properties after heating is shown in Figure 23 which displays the range of ratios found by dividing the mechanical properties of heated specimens by those of their respective non-heated specimens.

Table 2. Flexure and Compression Test Results Summary

Specimen	Maximum					Avg. Compression [psi]
	Load [lb]	Third-Point Displacement [in]	Stiffness [psi]	Moment [lb-in]	Modulus of Rupture [psi]	
H-1	3878	0.0334	160511	7755	719	19664
H-2	4479	0.0336	173738	8957	822	28795
H-3	4760	0.0373	179743	9520	912	21987
H-4	4699	0.0398	172658	9398	876	21909
H-5	5418	0.0392	171861	10837	1009	19608
H-6	5390	0.0395	176094	10781	1021	28881
H-7	4655	0.0356	165815	9309	868	29042
NH-1	5067	0.0387	180938	10134	930	12213
NH-2	4685	0.0363	163275	9369	887	17320
NH-3	4429	0.0300	189356	8858	851	14380
NH-4	2872	0.0285	150007	5744	539	14711
NH-5	3755	0.0291	163676	7511	712	14096
NH-6	3509	0.0309	142749	7018	661	18997
NH-7	2905	0.0248	145136	5810	538	18771

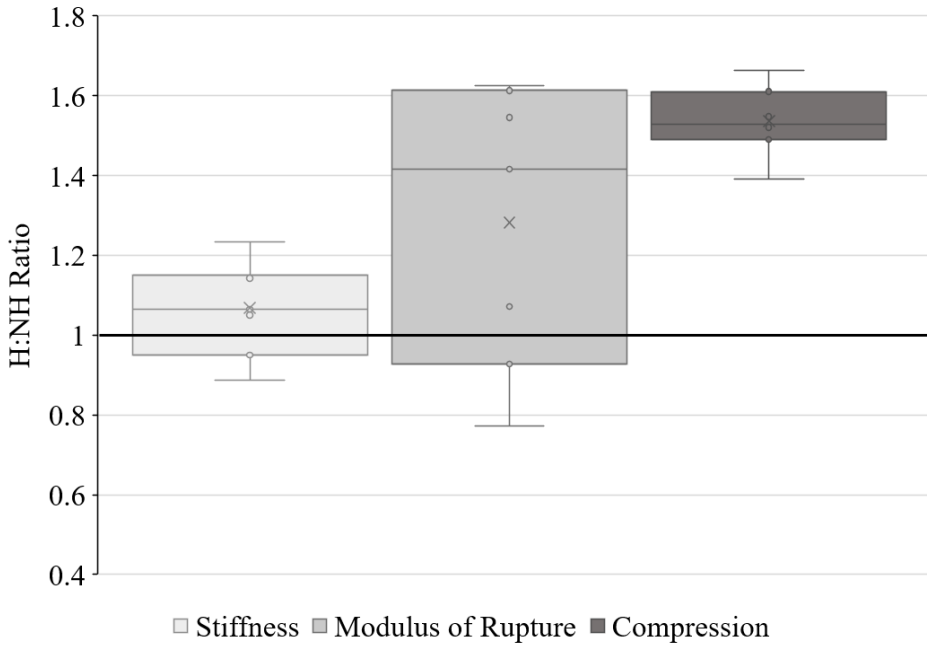

Figure 23. Ratio of mechanical properties of heated and non-heated specimens

4.2 Effect of Heat on UHPC Modulus of Rupture and Stiffness

Specimens heated to 250 °C show, on average, an increase in modulus of rupture (directly related to flexural capacity) and stiffness (Figures 24 and Figure 25). This indicates that this concrete mix could be suitable for use in Fe-SMA prestressing applications. Although the flexural capacity and stiffness of heated specimens were typically higher than their respective non-heated specimens, the heated specimens did show evidence of increased microcracking. This can be seen in the fracture planes of heated and non-heated specimens (Figure 26).

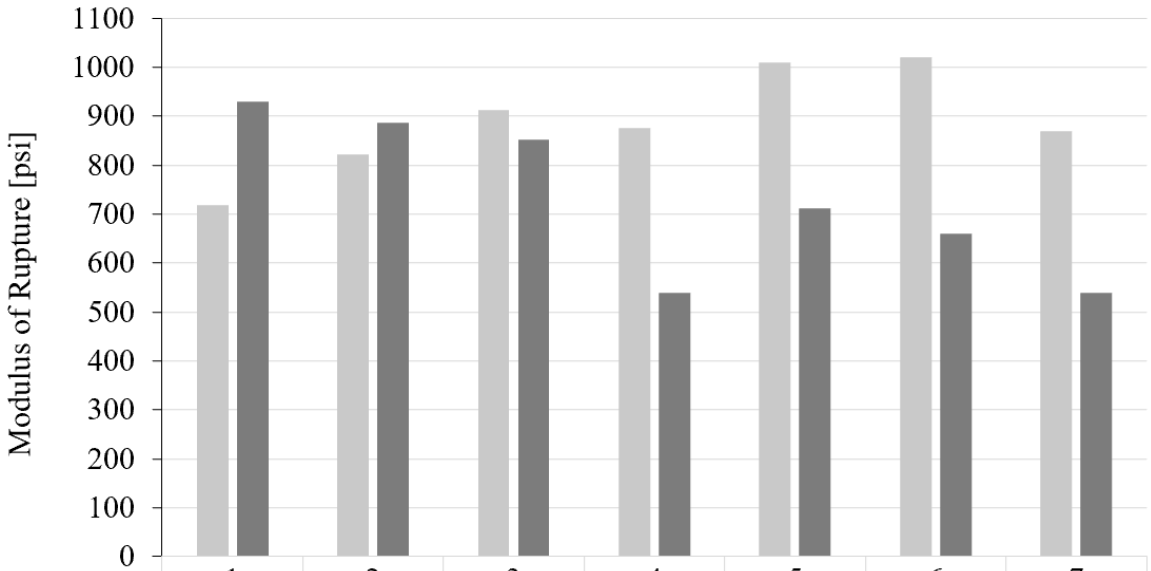

	1	2	3	4	5	6	7
Heated	719	822	912	876	1009	1021	868
Non-Heated	930	887	851	539	712	661	538

Figure 24. Modulus of rupture of heated and non-heated 4 by 4 by 16 in. flexure specimens

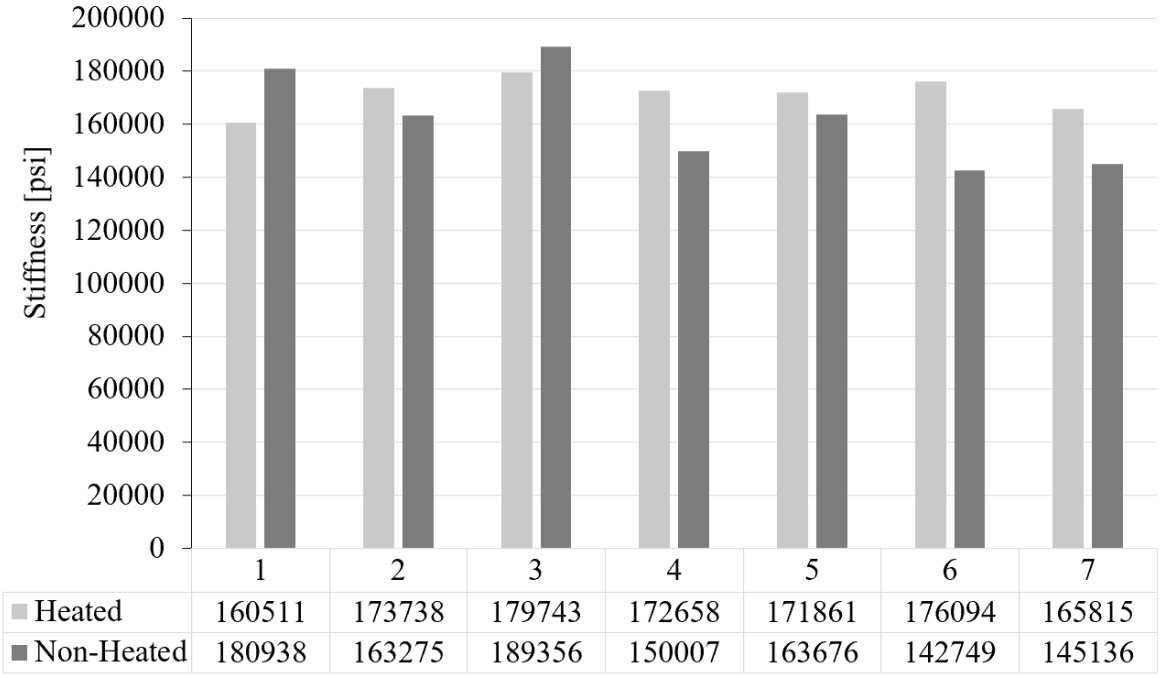

	1	2	3	4	5	6	7
Heated	160511	173738	179743	172658	171861	176094	165815
Non-Heated	180938	163275	189356	150007	163676	142749	145136

Figure 25. Stiffness of heated and non-heated 4 by 4 by 16 in. flexure specimens

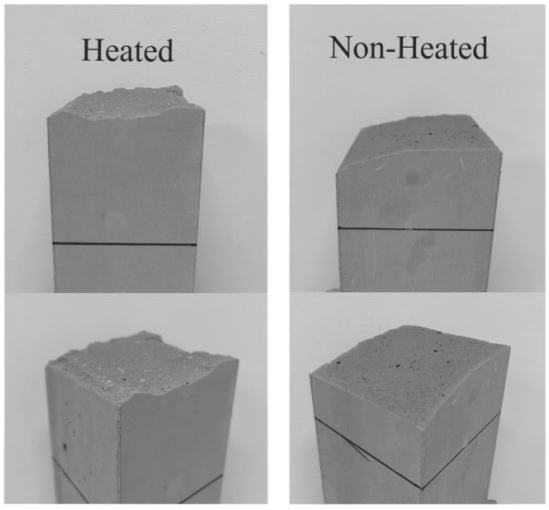

Figure 26. Typical fracture planes of heated and non-heated flexure specimens

Heated specimens consistently had more jagged fracture planes than the non-heated specimens. The increased roughness is assumed to correlate with increased microcracking. Microcracks are oriented randomly and easily propagated by tensile stresses. When a flexural

break occurs (in a specimen with substantial microcracking) the crack will likely follow the preexisting microcracks resulting in a jagged fracture plane (when compared to a specimen with less microcracking). This study assumes that the cement rehydration from evaporated free water provided enough of a strength increase to counteract the negative effects of microcracking within heated specimens.

4.3 Effect of Heat on UHPC Compressive Strength

Compression tests show that heating specimens consistently increases overall compressive strength (Figure 27) by an average of approximately 54% (Figure 23). The increase in compressive strength is likely due to cement rehydration by free water that is evaporated during heating. The compressive behavior of this mix upon heating is favorable for Fe-SMA prestressing because an increase in concrete compressive strength would help offset the relative decrease in compressive strength (due to the prestressing effect of Fe-SMA fibers putting the concrete in compression prior to loading).

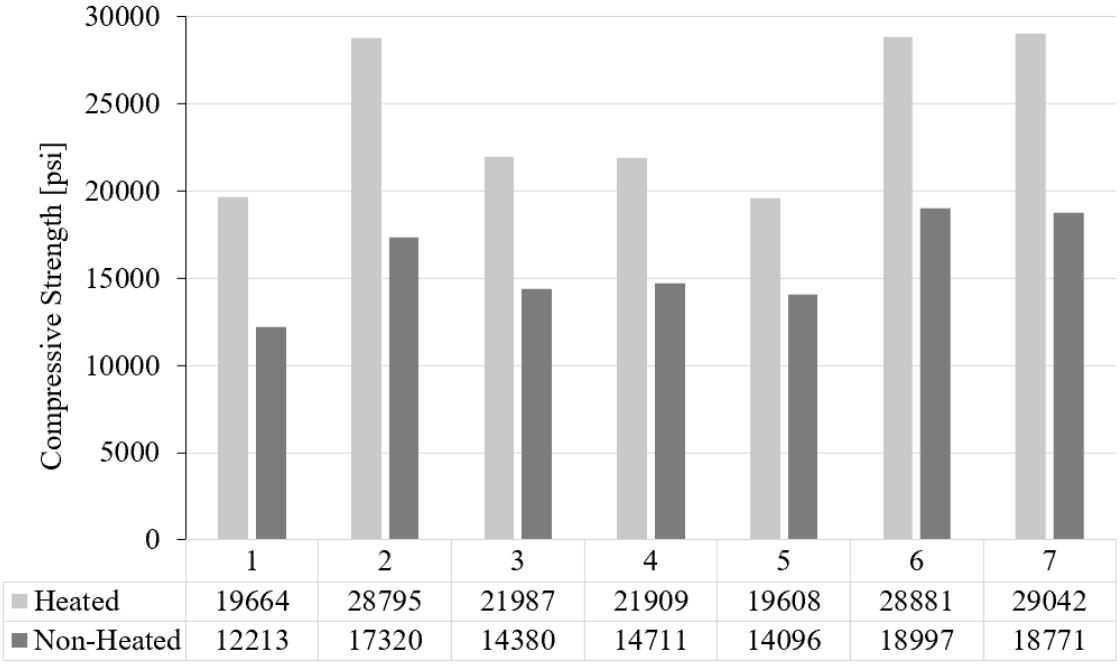

	1	2	3	4	5	6	7
Heated	19664	28795	21987	21909	19608	28881	29042
Non-Heated	12213	17320	14380	14711	14096	18997	18771

Figure 27. Compressive strength of heated and non-heated 2 by 2 by 2 in. concrete cubes

4.4 Effect of Heat on Fiber-to-Concrete Bond Strength

Steel fiber pull-out tests indicate that heating this concrete may increase fiber-to-concrete bond strength. Samples with embedment depths of 0.50 and 0.75 in. showed an increase in bond strength upon heating (Figure 28). This increase in bond strength is assumed to be attributed to the above-mentioned increase in UHPC strength from heating. Heated and non-heated samples with an embedment depth of 0.25 in. showed little difference in average bond strength, but the variance of heated specimens was almost two times greater (Figure 28). The similarity in bond strength may be due to the short embedment preventing the steel fiber from fully engaging with the surrounding concrete. Therefore, the tensile and compressive strength of the concrete may have less of an effect on pull-out resistance. The increased variance could be caused by the presence of heat induced cracking along the bond. A crack at this interface would have a greater effect on total bond strength than a crack of the same size in a sample with a deeper embedment.

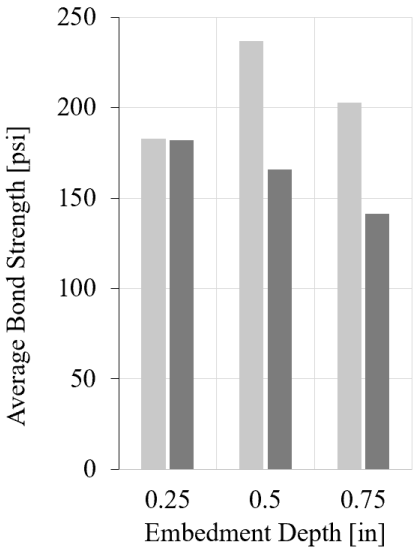

		Standard Deviation
Heated	0.25	35.9
	0.5	6.8
	0.75	8.1
Non-Heated	0.25	18.0
	0.5	14.6
	0.75	7.1

Figure 28. Fiber-to-concrete bond strength test results

Using Equation 10, (with a recovery stress of 50ksi and a bond strength of 200 psi) Fe-SMA fiber length would need to be at least 4.9 inches to adequately transfer recovery stress from the fibers to the UHPC. This fiber length could cause issues with workability and make fibers more prone to bending while mixing. Bent Fe-SMA fibers could try to straighten upon heating which may cause undesired internal tensile stress within the concrete [8]. To practically prestress UHPC with Fe-SMA fibers, geometric anchorage should be provided to allow for a reduction in fiber length while maintaining adequate stress transfer.

4.5 Validation of Fe-SMA Achievable Recovery Stress

The results of the Fe-SMA material behavior test indicate that a recovery stress of approximately 50 ksi is achievable (Figure 29). Using Equation 6, this would result in concrete prestress of about 354 psi for every 1% (per volume) of Fe-SMA fibers added to a UHPC mix (Table 3). Future studies should investigate the effect of Fe-SMA fiber content on prestress as

the increase in prestress with fiber content may not be linear after a certain quantity of fibers have been added.

Table 3. Estimation of achievable prestress

Fe-SMA fiber content by volume	Concrete Prestress [psi]
1%	354
2%	707
3%	1061
4%	1414

Thermocouple wires measured a maximum temperature of approximately 250 °C, but it is believed that the actual temperature within the Fe-SMA rod was closer to 218 °C. The high reading is likely due to a temperature spike (Figure 29) within the thermocouple wire (caused by insufficient wire insulation). Although the target temperature of 250 °C was not reached, the results of this test do indicate that this Fe-SMA can produce a recovery stress great enough to prestress concrete. Additionally, because recovery stress typically increases with an increase in activation temperature [4,2] it can be assumed that, with an activation temperature of 250 °C, recovery stress would be higher than the value found.

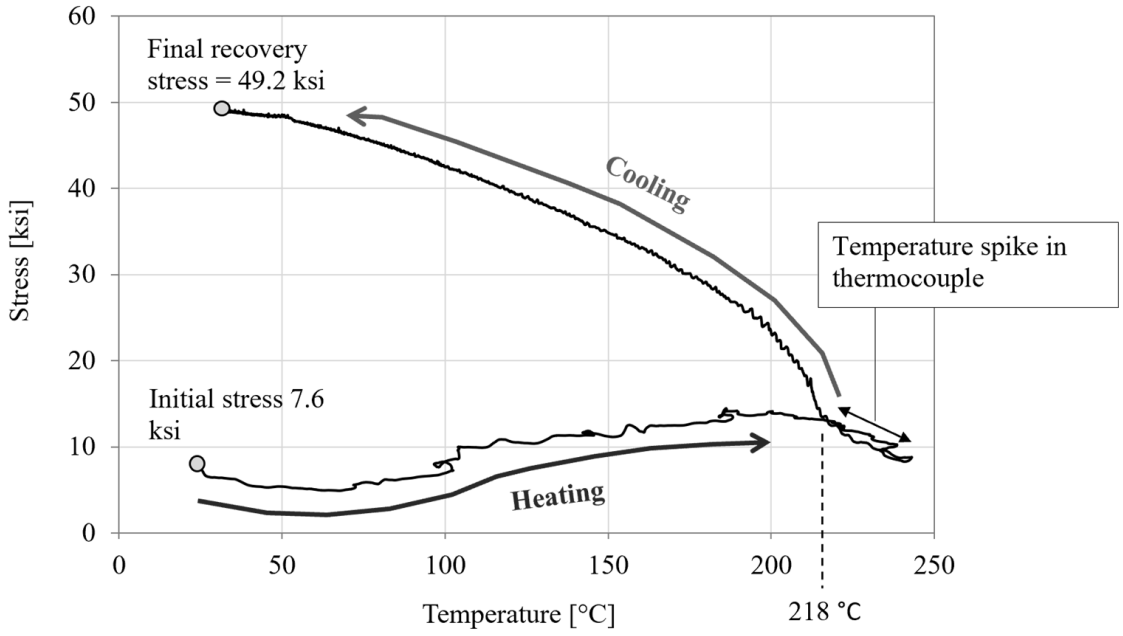

Figure 29. Recovery stress development

5 Conclusions and Future Research

1. The Fe-SMA displayed a recovery stress of approximately 50 ksi which could prestress concrete 354 psi for every 1% (by volume) of Fe-SMA fibers added to a mix. Because the actual activation temperature is believed to have been closer to 218 °C, the recovery stress of the Fe-SMA, when heated to 250 °C, would likely be exceed 50 ksi and allow more efficient prestressing.

2. The Ductal premix used for this study was found to have a behavior after heating that is favorable for Fe-SMA prestressing applications. When heated this UHPC (on average) showed increases in modulus of rupture, compressive strength, steel fiber-to-concrete bond strength, and stiffness. The use of this mix in future Fe-SMA prestressing research is recommended. Additionally, the behavior of this mix when exposed to lower SMA activation temperatures could be explored to determine an optimal Fe-SMA activation temperature.

3. Some form of geometric anchorage should be provided to allow for a reduction in fiber length while maintaining adequate stress transfer from the fibers to the concrete. Assuming Fe-SMA fiber-to-concrete bond strength is similar to the steel fiber-to-concrete bond strength found, the length of fiber required to effectively transfer recovery stress may be too great for practical applications. Future research should investigate various forms of geometric anchorage for Fe-SMA fibers within UHPC.

4. In later research, UHPC specimens with varying quantities of Fe-SMA short fibers should be fabricated and tested in flexure. This could verify the concept of prestressing with Fe-SMA short fibers and facilitate the development of a more accurate method of estimating achievable prestress based on fiber content. Additionally, this may shed light on factors that could cause prestress loss such as concrete creep, shrinkage, and elastic shortening.

6 References

1. American Institute of Steel Construction, (AISC) (2017). "Steel Construction Manual." AISC, Chicago.

2. Choi, E., Ostadrahimi, A., Kim, W. H., & Seo, J. (2021). Prestressing effect of embedded Fe-based SMA wire on the flexural behavior of mortar beams. *Engineering Structures*. https://doi.org/10.1016/j.engstruct.2020.111472

3. Czaderski, Weber, Shahverdi, Motavalli, Leinenbach, Lee, Rolf, Michels 'Iron-based shape memory alloys (Fe-SMA) - a new material for prestressing concrete structures' SMAR 2015

4. Hong, K., Lee, S., Han, S. H., & Yeon, Y. (2018). Evaluation of Fe-Based Shape Memory Alloy (Fe-SMA) as Strengthening Material for Reinforced Concrete Structures. *Applied Sciences*, *8*(5), 730. https://doi.org/10.3390/app8050730

5. Lee, W. H., Weber, B., Feltrin, G., Czaderski, C., Motavalli, M., & Leinenbach, C. (2013). Phase transformation behavior under uniaxial deformation of an Fe–Mn–Si–Cr–Ni–VC shape memory alloy. *Materials Science and Engineering A-Structural Materials Properties Microstructure and Processing*, *581*, 1–7. https://doi.org/10.1016/j.msea.2013.06.002

6. Ma, Q., Guo, R., Zhao, Z., Lin, Z., & He, K. (2015). Mechanical properties of concrete at high temperature—A review. *Construction and Building Materials*, *93*, 371–383. https://doi.org/10.1016/j.conbuildmat.2015.05.131

7. Moser, K., Bergamini, A., Christen, R. *et al.* 'Feasibility of concrete prestressed by shape memory alloy short fibers.' *Mat. Struct.* **38,** 593–600 (2005). https://doi.org/10.1007/BF02479551

8. Orvis, Jansen 'Prestressing Concrete with Shape Memory Alloy Fibers' California Polytechnic State University, San Luis Obispo 2009

9. Prinz, G. S., & Murray, C. D. (2021). On the pullout strength of human nasal hair. *Materialia*, *16*, 101102. https://doi.org/10.1016/j.mtla.2021.101102

10. Xue, C., Yu, M., Xu, H., Xu, L., & Saafi, M. (2022). Compressive performance and deterioration mechanism of ultra-high performance concrete with coarse aggregates under and after heating. *Journal of Building Engineering*, *64*. https://doi.org/10.1016/j.jobe.2022.105502.

11. Yang, J., Peng, G. F., Zhao, J., & Shui, G. (2019). On the explosive spalling behavior of ultra-high performance concrete with and without coarse aggregate exposed to high temperature. *Construction and Building Materials*, *226*, 932–944. https://doi.org/10.1016/j.conbuildmat.2019.07.299